Optimal use of land surface temperature data to detect changes in tropical forest cover

Thijs T. van Leeuwen,[1,2] Andrew J. Frank,[3] Yufang Jin,[1] Padhraic Smyth,[3] Michael L. Goulden,[1] Guido R. van der Werf,[2] and James T. Randerson[1]

Received 26 July 2010; revised 31 December 2010; accepted 18 January 2011; published 15 April 2011.

[1] Rapid and accurate assessment of global forest cover change is needed to focus conservation efforts and to better understand how deforestation is contributing to the buildup of atmospheric CO_2. Here we examined different ways to use land surface temperature (LST) to detect changes in tropical forest cover. In our analysis we used monthly 0.05° × 0.05° Terra Moderate Resolution Imaging Spectroradiometer (MODIS) observations of LST and Program for the Estimation of Deforestation in the Brazilian Amazon (PRODES) estimates of forest cover change. We also compared MODIS LST observations with an independent estimate of forest cover loss derived from MODIS and Landsat observations. Our study domain of approximately 10° × 10° included the Brazilian state of Mato Grosso. For optimal use of LST data to detect changes in tropical forest cover in our study area, we found that using data sampled during the end of the dry season (~1–2 months after minimum monthly precipitation) had the greatest predictive skill. During this part of the year, precipitation was low, surface humidity was at a minimum, and the difference between day and night LST was the largest. We used this information to develop a simple temporal sampling algorithm appropriate for use in pantropical deforestation classifiers. Combined with the normalized difference vegetation index, a logistic regression model using day-night LST did moderately well at predicting forest cover change. Annual changes in day-night LST decreased during 2006–2009 relative to 2001–2005 in many regions within the Amazon, providing independent confirmation of lower deforestation levels during the latter part of this decade as reported by PRODES.

Citation: van Leeuwen, T. T., A. J. Frank, Y. Jin, P. Smyth, M. L. Goulden, G. R. van der Werf, and J. T. Randerson (2011), Optimal use of land surface temperature data to detect changes in tropical forest cover, *J. Geophys. Res.*, *116*, G02002, doi:10.1029/2010JG001488.

1. Introduction

[2] The clearing of humid tropical forest has important consequences for ecosystem function [*DeFries et al.*, 2004; *Foley et al.*, 2005], regulation of regional [*Nobre et al.*, 1991] and global climate [*Shukla et al.*, 1990; *Bala et al.*, 2007], water resources [*Hamilton and King*, 1983], biogeochemical cycles [*Houghton*, 1991], biological diversity [*Sala et al.*, 2000], and the maintenance of soil fertility [*Andreux and Cerri*, 1989; *Davidson et al.*, 2007]. Substantial improvements in the quantification of tropical forest cover losses have been made during the last decade [*Houghton et al.*, 2000; *Achard et al.*, 2002; *Instituto Nacional de Pesquisas Espaciais* (*INPE*), 2002; *DeFries et al.*, 2002; *Food and Agriculture Organization*, 2006; *Hansen et al.*, 2008], and with the likelihood of new climate agreements including Reducing Emissions from Deforestation and Degradation (REDD) [*United Nations Framework Convention for Climate Change*, 2005] there will be an even greater need for accurate forest monitoring methods, particularly for approaches that enable monitoring in near real time [e.g., *Morton et al.*, 2005]. This information is required to better understand land use change effects on the global carbon cycle [*Canadell et al.*, 2007], and to gauge the success of mitigation activities involving forests [*Nabuurs et al.*, 2007]. A primary challenge in estimating contemporary rates of forest cover loss is to efficiently extract information from different satellite products at multiple spatial and temporal resolutions and then to combine this information in an effective way with ground-based observations [*Achard et al.*, 2007; *Goetz et al.*, 2009; *DeFries et al.*, 2007].

[3] To map changes in tropical forest cover, often a first step is to classify land cover types, including different types

[1]Department of Earth System Science, University of California, Irvine, California, USA.
[2]Department of Hydrology and Geo-environmental Sciences, VU University Amsterdam, Amsterdam, Netherlands.
[3]Department of Computer Science, University of California, Irvine, California, USA.

0148-0227/11/2010JG001488

of forest, savanna, and agriculture. Surface reflectances in the visible and near infrared, and vegetation indices (VI), which are linear or nonlinear combinations of the reflectance in two or more bands, are frequently used as metrics in land cover classification algorithms [e.g., *DeFries and Townshend*, 1994; *Los et al.*, 1994]. Annual time series of the normalized difference vegetation index (NDVI), based on AVHRR data, were used by *DeFries and Townshend* [1994] to develop global land cover maps with a 1° spatial resolution. As global AVHHR data became available at higher resolution [*Eidenshink and Faundeen*, 1994], land cover maps with a finer spatial resolution (8 km and 1 km) were created [*DeFries et al.*, 2000; *Hansen and DeFries*, 2004]. The accuracy of land cover change estimates has been further enhanced by the development and application of more sophisticated classification algorithms, including decision trees [*Hansen et al.*, 2000; *Friedl and Brodley*, 1997], neural networks [*Gopal and Woodcock*, 1996], and mixture models [*DeFries et al.*, 1995; *Anderson et al.*, 2005]. In several different studies fractional cover images derived from mixture models have been used successfully for monitoring deforestation [*Shimabukuro et al.*, 1998] and land cover change [*Carreiras et al.*, 2002].

[4] Although surface reflectance observations and VIs are widely used in assessments of forest cover, additional information can be extracted from thermal infrared bands. Land surface temperature (LST) during the day, derived from thermal infrared bands, has been shown to be closely related with the density of the canopy across different vegetation types [*Price*, 1984; *Smith and Choudhury*, 1991; *Nemani and Running*, 1997] and therefore helpful in classifying land cover types [*Lambin and Ehrlich*, 1995; *Nemani and Running*, 1997; *Roy et al.*, 1997]. *Borak et al.* [2000] confirmed the importance of LST data as a complementary source of information to the NDVI data. In more recent studies the daytime land LST product of the MODIS Terra satellite has been included in algorithms for detecting forest cover change in the humid tropics [e.g., *Hansen et al.*, 2008]. The information content of LST, however, has not been systematically evaluated [*Mildrexler et al.*, 2007]. Key uncertainties remain with respect to how the effectiveness of LST information varies seasonally and how it compares with information derived from visible and near infrared wavelengths.

[5] Changes in land cover influence LST by means of several different pathways [e.g., *Carlson and Gillies*, 1994; *Friedl*, 2002; *Pongratz et al.*, 2006]. LST is regulated by the amount of shortwave radiation absorbed by the surface (i.e., surface albedo), surface conductance, the amount of water available for evaporative cooling, wind speed, and surface roughness which regulates the strength of both sensible and latent heat fluxes. During the dry season, daytime LST has been shown to be linearly related to the density of the canopy across different vegetation types [*Nemani et al.*, 1993]. Areas of tree cover, which often have deeper roots and thus may access greater water resources, tend to have higher rates of evapotranspiration (and thus lower LSTs) during the dry season than grasses and other herbaceous cover that may senesce. Increases in LST in deforested areas may be further amplified by reductions in roughness length that reduce the dissipation of energy by means of either sensible or latent heat fluxes. Different model experiments in the state of Mato Grosso, Brazil, conducted by *Pongratz et al.* [2006] confirm that day LST increases in areas with lower forest cover, particularly during the dry season for pastures, compared with dense forest.

[6] Night LSTs are also sensitive to forest cover. Nocturnal drainage of air from upper canopy layers and pooling of cold air at the forest floor keeps upper levels of the canopy relatively warm [*Goulden et al.*, 2006]. This process of nocturnal cold air drainage and pooling cannot take place in short stature vegetation; net loss of thermal radiation cools the land surface during the night, but the colder air that is created from interaction with the canopy remains at the surface and in contact with the canopy elements that are emitting thermal radiation. Satellite sensors only measure the temperature of the top of forest canopies, so intact forest shows a higher night LST than comparable areas with short-stature vegetation [*Goulden et al.*, 2006]. Considering both day and night LSTs, differences in the diurnal temperature range are expected to be smaller for forests and larger for grasslands and shrublands, given the biophysical processes described above [*Collatz et al.*, 2000]. Within Mato Grosso, *Pongratz et al.* [2006] found, for example, that the diurnal temperature range increases by over 7°C when forests are converted to bare ground.

[7] Here we explored the use of LST data from the MODIS land surface climate modeling grid (CMG) product for quantifying forest cover and its change, and compared our findings to PRODES estimates of deforestation losses in the state of Mato Grosso, Brazil. We assessed how the information content of LST as a predictor of forest cover changed seasonally and also as a function of day, night, and day-night LST differences. Based on this analysis, we developed a metric to monitor forest cover change in the humid tropics. Several experiments were performed to further test the ability of day LST, night LST, and day-night LST differences during different seasonal periods for forest cover mapping by ingesting them one by one in a logistic regression model. We found that effective use of the LST data required identifying the optimal seasonal period within each region when water vapor in the atmosphere was minimal and drought stress was greatest. Our study demonstrated the usefulness of MODIS LST data at a coarse spatial resolution for the rapid identification of deforestation hot spots and for assessing regional trends.

2. Methods

2.1. Study Area

[8] Our study area encompassed the state of Mato Grosso, Brazil (7.0°–19.0°S, 62.0°–50.0°W) (Figure 1a). Evergreen broadleaf forest was the dominant plant functional type (pft) in the northern part of the state. Woodland savanna (cerrado), savanna, and agriculture pfts were more abundant in the southern and eastern part of the domain (Figure 1b). One of the largest contiguous tracts of forest in Mato Grosso occurs within the Xingu Indigenous Reserve, located in the northeastern part of the state (red line in Figure 1b). One of the world's largest wetlands, the Pantanal, is located in the south central part of the domain (gray line in Figure 1b).

[9] Located within the "arc of deforestation," the state of Mato Grosso has experienced rapid changes in land cover because of agricultural expansion and intensification [*Morton*

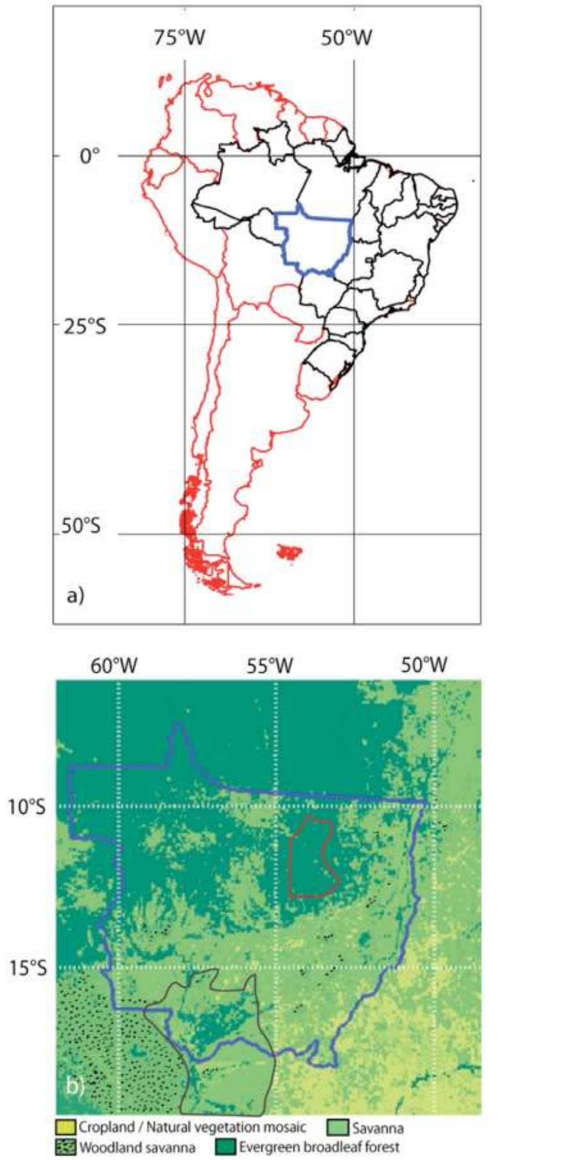

Figure 1. (a) The spatial domain of our analysis included the state of Mato Grosso, Brazil. (b) Evergreen broadleaf forests were the dominant land cover type in the northern part of the domain. Toward the south and east, woodland savannas, savannas, and agriculture land cover classes were increasingly abundant. The perimeters of the Pantanal and Xingu Indigenous Reserve are indicated by the gray and red lines, respectively. These observations are from the MODIS Land Cover Product MOD12C1 [*Friedl et al.*, 2002] for the year 2004 and with a spatial resolution of 0.05° × 0.05°.

et al., 2006]. The two most dominant forms of land cover change in Mato Grosso during 2001–2004 were forest conversion to pasture and forest conversion to cropland, accounting for approximately 65% and 20%, respectively, of all observed land cover transitions [*Morton et al.*, 2006]. Areas previously cleared for cattle ranching were also observed to undergo subsequent conversion to soybean agriculture (agricultural intensification), and to a lesser extent, to corn, cotton and sugarcane agriculture. Remaining forest and woodland savanna in central, eastern, and southern Mato Grosso may be vulnerable to further change as a result of continued expansion of mechanized agriculture [*Jasinski et al.*, 2005]. The large mechanized clearings that are used for the creation of pastures and croplands in the study area are more easily detected by the coarse resolution products presented in this study.

2.2. Data

2.2.1. MODIS LST and NDVI

[10] We obtained LST and NDVI products from the Moderate Resolution Imaging Spectroradiometer (MODIS [*Salomonson et al.*, 1989]), on board NASA's Terra satellite (nominal 10.30 A.M. descending and 10:30 P.M. ascending equatorial crossing times). We used data from MODIS Terra (instead of Aqua) because our initial focus was on the 2000–2005 period; this allowed us to make direct comparisons with the *Hansen et al.* [2008] deforestation estimates described below.

[11] For LST we used the collection 5 monthly level-3 MOD11C3 product described by Z. Wan (MODIS Land Surface Temperature Products Users' Guide, http://www.crseo.ucsb.edu/modis/LstUsrGuide/MODIS_LST_products_Users_guide_march06.pdf, 2006). This product provides monthly composited and averaged temperature and emissivity values at a 0.05° geographic climate modeling grid (CMG), as well as the averaged observation times and viewing zenith angles for daytime and nighttime LSTs. The product is derived from the daily MOD11C1 product that has a 0.05° × 0.05° spatial resolution, which is, in turn, based on a reprojection and average of the MOD11B1 product.

[12] Validation of the MOD11C3 product has occurred through a series of field campaigns conducted in 2000–2006 and over more locations and time periods through radiance-based validation studies [*Wan et al.*, 2002]. Clouds prevent surface thermal infrared radiation from reaching the satellite, and therefore the MODIS LST data are only available for clear-sky conditions. We created a spatial subset over the 12° × 12° region (240 × 240 grid cells) of our study domain using all available data from March 2000 through December 2005. We also compared changes in LST during two separate periods: 2001–2005 and 2006–2009 to test whether recent decreases in deforestation reported by PRODES are consistent with the LST observations.

[13] For NDVI we used the monthly Level-3 MOD13C2 product that was reprojected on a 0.05° geographic CMG [*Huete et al.*, 2002]. The data are spatial and temporal composites of the cloud-free gridded MODIS NDVI data that are provided every 16 days at a 1 km resolution (MOD13A2). The historical MODIS NDVI climatology record is used to fill those pixels without any cloud-free observations to achieve cloud-free global coverage.

[14] The MODIS NDVI algorithm operates on a per-pixel basis and ingests multiple level-2 daily atmospherically corrected surface reflectances to generate a composited NDVI (A. Huete et al., *MODIS Vegetation Index (MOD13): Algorithm Theoretical Basis Document*, http://modis.gsfc.nasa.gov/data/atbd/atbd_mod13.pdf, 1999). It first filters the data based on quality, cloud and viewing geometry. Observations that are contaminated by residual atmospheric effect and extreme off-nadir views are considered as low quality data. Only the higher quality and cloud-free filtered

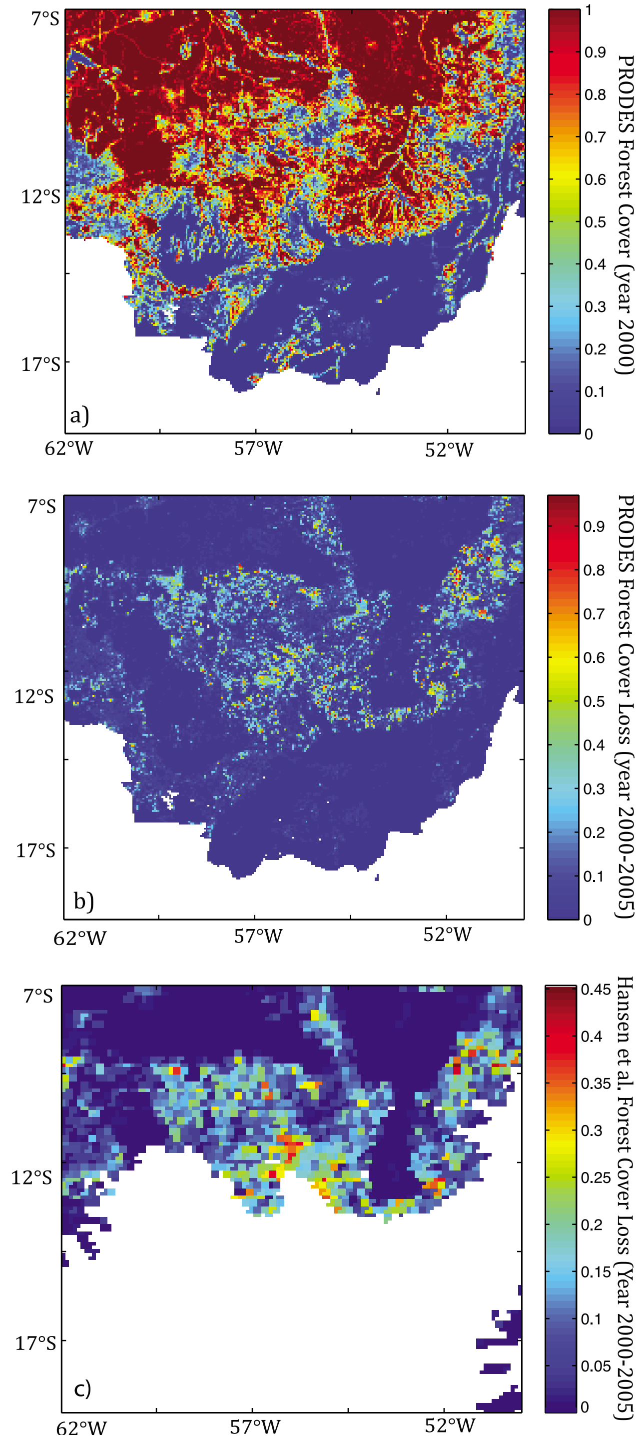

Figure 2. (a) Forest cover in Mato Grosso for the year 2000 from the Program for the Estimation of Deforestation in the Brazilian Amazon (PRODES [*INPE*, 2002]). The original PRODES data were resampled to a geographic 0.05° × 0.05° grid and are shown here as a fraction of total forest cover between 0 and 1. White pixels correspond to the area outside the PRODES domain. (b) Forest cover loss between the years 2000 and 2005 from PRODES. (c) Forest cover loss between the years 2000 and 2005 in Mato Grosso from *Hansen et al.* [2008]. White pixels correspond to the area outside the Hansen et al. humid tropical forest cover change domain.

data are retained for temporal compositing. The two highest NDVI values during each 16 days are then compared and the one closest to nadir view is selected. This constrained view-angle composite method reduces the spatial and temporal inconsistency due to angular variations encountered in the traditional maximum value composite (MVC) [*Holben*, 1986].

2.2.2. PRODES Forest Cover

[15] The Program for the Estimation of Deforestation in the Brazilian Amazon (PRODES) is one of the largest forest monitoring projects in the world [*INPE*, 2002]. The PRODES deforestation product is generated from the analysis of high-resolution Landsat Thematic Mapper (TM) images by the Brazilian Instituto Nacional de Pesquisas Espaciais (National Institute for Space Research, INPE). Areas of deforestation of more than 6.5 ha can be detected. The first digital mapped version was created in 1997, and since 2000 the product has been produced annually with a time delay of approximately 5 months after the end of each calendar year. The PRODES data set covers the Brazilian Amazon.

[16] PRODES data that we used in this study were downloaded at 90 m resolution in GeoTiff format from the INPE website (http://www.obt.inpe.br/prodes/). To reproject the PRODES observations onto the same geographic grid as the MODIS observations, we first converted the PRODES GeoTiff image to a vector (polygon) format using ArcGIS software. We then reprojected these polygons from Datum SAD69 to WGS84 using the SAD_1969_To_WGS_1984_1 geographic transformation method that yielded a registration error that was less than 10m. The final reprojected and regridded PRODES forest cover product for 2000 is shown in Figure 2a. Forest cover loss between the years 2000 and 2005 is shown in Figure 2b. With the base map of forest cover in 2000 and the increments of annual deforestation, we also calculated the forest cover for each year during 2000–2005.

2.2.3. *Hansen et al.* [2008] Forest Cover Loss

[17] Besides the PRODES data set, we included a comparison between LST derived forest cover and forest cover change with the forest cover loss data set of *Hansen et al.* [2008]. This data set represents gross forest cover loss for the humid tropical forest biome between the year 2000 and 2005. MODIS and Landsat data were combined to estimate areas where forest clearing occurred. Moderate resolution MODIS data were used to identify areas of likely forest cover loss and to stratify the humid tropics into regions of low, medium, and high probability of forest clearing. Various samples sized 18.5 km × 18.5 km were taken within these areas, and interpreted for forest cover and forest clearing by using high spatial resolution Landsat imagery from 2000 and 2005. A more detailed description of the data set is given by *Hansen et al.* [2008].

[18] The humid tropical forest cover loss data that we used in this study were downloaded in a sinusoidal GeoTiff format at 18.5 km × 18.5 km spatial resolution from the Global Forest Monitoring website of South Dakota State University (http://globalmonitoring.sdstate.edu). To reproject the *Hansen et al.* [2008] data set onto the same geographic grid as the MODIS observations, we followed the procedure as with converting PRODES data, as described in section 2.2.2. *Hansen et al.* [2008] forest cover loss for our study area between the years 2000 and 2005 is shown in Figure 2c.

2.2.4. Precipitation and Relative Humidity

[19] In this study we used the Tropical Rainfall Measuring Mission (TRMM) 3B43 product to estimate precipitation within our study domain. The TRMM 3B43 algorithm uses four different independent data streams to produce the best estimate precipitation rate (mm/h) and root-mean-square (RMS) precipitation error estimates [*Kummerow et al.*, 1998]. These data have a spatial resolution of 0.25° × 0.25° and a monthly time step. We resampled the TRMM product during 2000–2005 at a spatial resolution of 0.05° × 0.05° to overlay on the LST and NDVI CMG grid.

[20] To estimate the relative humidity level at the surface (1000 hPa) in our study area, we used data from the AIRS instrument, on board of NASA's Aqua satellite. In our study we used the level 3 V5 monthly AIRX3STM product, with a spatial resolution of 1° × 1°. The product contains standard relative humidity (in %) for different pressure levels that is derived from observations from the Atmospheric Infrared Sounder (AIRS) and the Advanced Microwave Sounding Unit (AMSU) [*Aumann et al.*, 2003]. For this study we used the relative humidity data at 1000 hPa from the ascending orbit. These observations represent relative humidity during the day at a ~1:30 P.M. overpass time.

[21] The PRODES forest cover map for 2000, reprojected to the CMG (section 2.2.2), was used to separate forest and nonforest areas using a threshold of 0.5 fractional cover. Due to the coarse resolution of the AIRS product (1° × 1°) compared to the PRODES forest cover, only AIRS pixels that fell in the forest domain (forest cover greater than 0.5) were used to estimate mean surface humidity in the forest part of the domain. Relative humidity of the nonforest was calculated by using pixels that fell completely in the nonforest domain (forest cover less than or equal to 0.5). The AIRS product was available from August 2002 through the present, and for our analysis we constructed a mean annual cycle for years 2003–2005.

2.3. Logistic Regression

[22] We used a logistic regression model [*Hosmer and Lemeshow*, 2004] to relate MODIS LST and NDVI observations to per-pixel proportional forest cover. More precisely, we defined the model as

$$\ln\left(\frac{p_{it}}{1-p_{it}}\right) = \beta^T \mathrm{X}_{it} \tag{1}$$

where p_{it} is the fraction of forest cover for pixel i in year t according to PRODES (see section 2.2.2), X_{it} is a vector of MODIS observations for pixel i in year t, and β is a vector of model parameters (which are estimated from a set of training data). In the most general case we consider, the vectors X_{it} and β each have three components: the first corresponding to a constant intercept term, the second to a NDVI measurement, and the third to a LST measurement. The index i ranges over spatial pixels and the index t ranges over years. Each pixel i and year t provided one training data point, i.e., a X_{it} and p_{it} pair. To define a NDVI or LST X_{it}, we computed the mean values of the corresponding product either over a 12 month period from February to January, or for a locally defined 3 month period during the dry season or wet season (see section 3.3 for details). Given an estimated parameter vector β the model made predictions about proportional forest cover (e.g., at a future time t) according to:

$$p_{it} = \frac{1}{1+e^{-\beta^T \mathrm{X}_{it}}} \tag{2}$$

To estimate the parameters we used the traditional iteratively reweighted least squares (IRLS) algorithm for logistic regression [*Nelder and Wedderburn*, 1972]. This algorithm corresponds to a Newton-Raphson optimization of the likelihood function. The vector β is computed such that the likelihood of the training data is maximized and then used in equation (2) to make predictions of forest cover in the test data. Since we were interested in the forest cover change (i.e., deforestation and forest regrowth), we made predictions both at the beginning and end of a period of interest and estimated changes in forest cover as the difference between the two predicted forest cover maps. We also evaluated an alternative approach where a logistic model was trained using differences in MODIS signals to predict differences in forest proportions more directly, but we found that this produced no significant difference in prediction accuracy compared to computing the difference of two predictions at different times.

[23] By evaluating the model's performance given several different sets of input features, we assessed the value of day LST, night LST, and day-night LST differences as metrics for detecting forest cover change. In each of our model experiments, we trained the model using data from years 2000 through 2004. We made predictions both for year 2000 and year 2005 to estimate the difference in forest cover between the two years. To evaluate model performance, we compared the estimated difference with the deforestation rates reported by PRODES. Note that PRODES does not include forest regrowth (an increase in forest cover between 2000 and 2005) whereas in the model these transitions were allowed.

[24] We ran a series of experiments varying the input feature data source (LST alone, NDVI alone, or both together), the time of day at which the LST data were collected (day, night, or day-night difference), and the sampling period for constructing the feature space (dry season, wet season, or 12 month mean). In our first experiment we restricted ourselves to dry season LST data and evaluated model performance for each of day, night, and day-night difference measurements. In our second experiment we used day-night difference LST data and examined the effect varying the sampling period. Next we trained the model using only the NDVI data, again for all three of the different sampling periods. Finally, we evaluated the model using day-night difference LST data together with NDVI, once again comparing all three sampling periods.

[25] For each experiment we computed several performance metrics to help compare the relative quality of the predictions. First, we considered the linear correlation between the predicted and actual forest cover change values over the entire region of study. We then considered the ratio of the predicted area versus actual change values: a value of 1 would be ideal, and values above or below 1 indicate that the model is either too sensitive or unresponsive, respectively, to changes in the input features. We also estimated the linear correlation between predicted and actual change values over the active deforestation domain: the

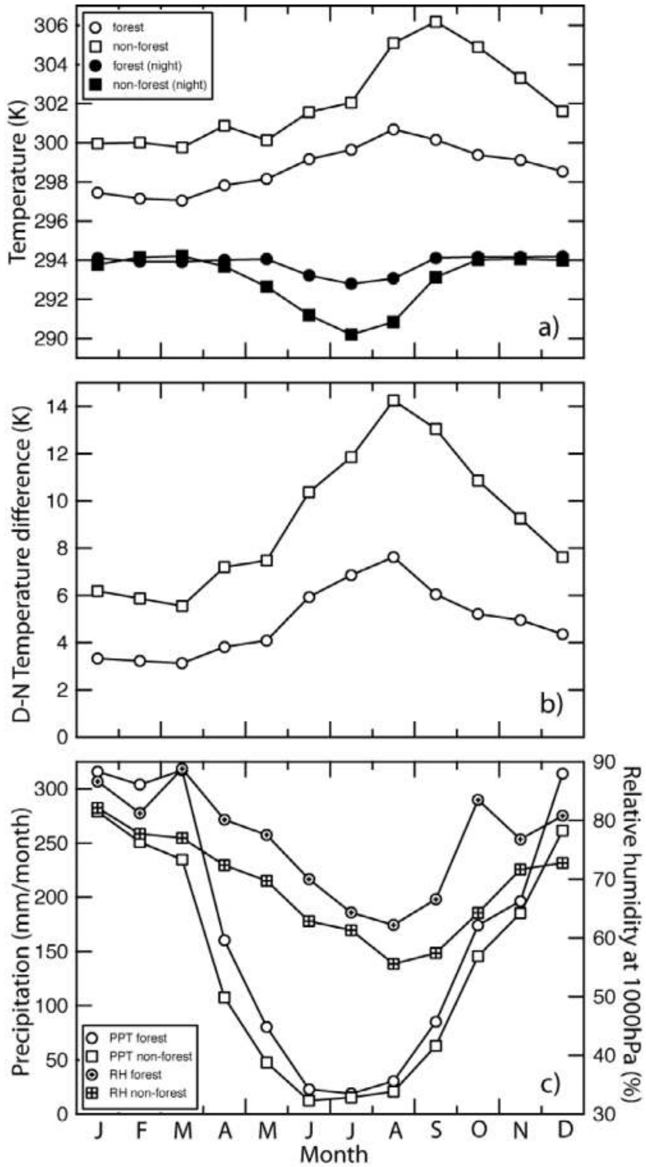

Figure 3. Surface temperatures, precipitation, and surface humidity for forest and nonforest parts of the study area. (a) Mean monthly day and night land surface temperatures (K) during 2000–2005 from the MODIS MOD3C11 product (Z. Wan, MODIS Land Surface Temperature Products Users' Guide, http://www.crseo.ucsb.edu/modis/LstUsrGuide/MODIS_LST_products_Users_guide_march06.pdf, 2006). (b) Same as Figure 3a, but for the mean monthly day-night temperature differences for forest and nonforest regions of the study area. The PRODES forest cover map (years 2000–2005) was used to separate forest and nonforest areas, using a threshold of 0.5 fractional cover. (c) Monthly mean precipitation (mm/month) during 2000–2005 from the TRMM 3B43 product [*Kummerow et al.*, 1998], and monthly relative humidity at 1000 hPa (in %) from the AIRS Level 3 V5 (AIRX3STM) Retrieval product. A mean for the years 2003–2005 was used.

subset of pixels for which PRODES indicates there was forest cover loss between 2000 and 2005. Finally, we computed the ratio of predicted to actual deforested area for the active deforestation domain.

3. Results

3.1. Spatial and Temporal Patterns of LST

[26] Mean daytime LST within the domain was substantially lower in forest areas than in nonforest areas throughout the year (Figure 3a). The monthly daytime temperature was at a maximum in August for forest areas (300.7K ± 1.2K (1σ)) and in September for nonforest areas (306.2K ± 2.2K). The largest forest-nonforest day LST differences occurred near the end of the dry season in August (4.4K), September (6.0K), and October (5.5K) (Figure 3a). The spatial distribution of LST was inversely related to forest area, as shown in Figure 4a. In August, the highest day LSTs, averaged during 2000–2005, occurred in nonforest areas in the southeastern part of the study area. The lowest LSTs occurred in forests in the northwest (Figure 4a).

[27] During night, forest areas in the north showed higher temperatures than those in the southern part of the study area, except for the wetlands of the Pantanal (Figure 4c). The annual cycle indicated that nonforest areas had more cooling at night than forest areas from May to September, with the greatest difference observed during July. The nighttime LST minimum within the domain occurred during the same months as the precipitation minimum, with a mean of 292.8 ± 0.5K for forest areas and 290.2K ± 1.4K for nonforest areas in July (Figure 3a). From October to April, when precipitation and surface humidity levels were high, nighttime temperatures were almost the same (around 294K) for forest and nonforest areas. This pattern may have been caused by decreased losses of longwave radiation (and thus decreased surface cooling) from high levels of column water vapor. In addition to the trapping of outgoing longwave radiation, higher soil moistures during the wet season may increase the heat capacity of the soils, further reducing the day-night surface temperature differences observed in grasslands and croplands [e.g., *Smith and Choudhury*, 1991; *Bruno et al.*, 2006]. The seasonal amplitude of LST was smaller in forest areas than that in nonforest areas for both day and night periods.

[28] Day-night LST differences were the largest toward the end of the dry season, with maxima during August of 7.6K ± 1.4K for forest areas and 14.2K ± 2.8K for nonforest areas (Figure 3b). A spatial map of the maximum day-night LST difference for August is shown in Figure 4e. In the southeastern part of our study area the largest day-night differences were observed. Smaller differences occurred in the northern forests and in the Pantanal region.

[29] Precipitation within the domain was at a minimum during June and July. In forest areas the minimum precipitation was in July with a mean of 18.9 mm/month (Figure 3c). The precipitation minimum in nonforest areas occurred a month earlier and had a lower mean (12.4 mm/month). Annually, forest areas received on average 24% more precipitation than nonforest areas. The 1–2 month time delay observed between minimum monthly precipitation and minimum monthly humidity may partly reflect increasing water stress throughout the dry season that caused decreases in

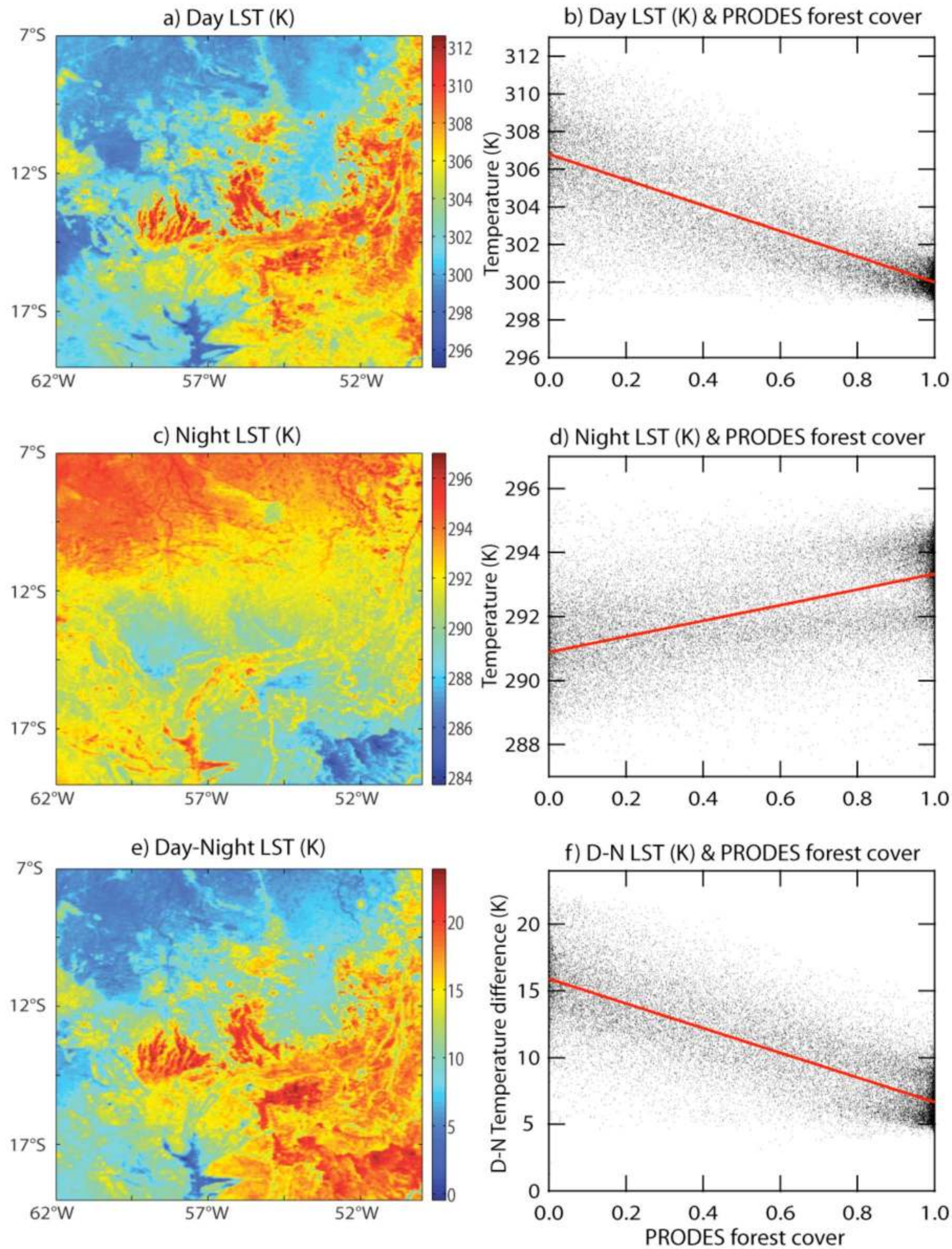

Figure 4. (left) Maps of (a) daytime LST (K), (c) nighttime LST, and (e) day-night LST difference in August (month of largest day-night LST difference), averaged during 2000–2005, and (right) their scatterplots versus forest cover from PRODES averaged over 2000–2005. Also shown in Figure 4 (right) are linear regression fits (solid line) of (b) daytime LST, (d) nighttime LST, and (f) day-night difference as a function of PRODES forest cover. The regression statistics were: (1) for daytime LST, a slope of −6.8, intercept of 306.8, and $p < 0.01$; (2) for nighttime LST, a slope of 2.5, intercept of 290.9, and $p < 0.01$; (3) for the day-night LST difference, a slope of −9.3, intercept of 15.9, and $p < 0.01$. In total, 30436 pixels were used for the above regressions.

Table 1. Monthly Relationships Between Physical Properties, Land Surface Temperature, and Land Surface Temperature Change

	Physical Properties				Correlation With PRODES Forest Cover[a]			Correlation With PRODES Forest Cover Change[b]			Correlation With *Hansen et al.* [2008] Forest Cover Change[c]		
Month	Precipitation[d] (mm/month)	Day LST (K)	Night LST (K)	Day-Night LST (K)	Day LST	Night LST	Day-Night LST	Day LST	Night LST	Day-Night LST	Day LST	Night LST	Day-Night LST
Jan	291.7	299.1	293.9	5.2	−0.69	0.14	−0.66	−0.12	0.05	−0.15	−0.23	0.19	−0.20
Feb	269.1	299.0	294.7	4.3	−0.73	−0.05	−0.50	−0.11	−0.01	−0.01	0.06	−0.09	0.08
Mar	263.1	298.8	294.1	4.7	−0.71	−0.09	−0.58	−0.09	0.03	−0.02	−0.03	0.06	0.02
Apr	125.8	299.8	293.8	6.0	−0.75	0.10	−0.72	−0.14	0.05	−0.21	0.02	0.17	−0.11
May	58.8	299.4	293.1	6.3	−0.71	0.41	−0.75	−0.37	0.02	−0.22	−0.31	−0.08	−0.18
Jun	16.0	300.7	291.9	8.8	−0.78	0.57	−0.77	−0.45	0.19	−0.50	−0.35	0.16	−0.39
Jul	16.5	301.2	291.1	10.1	−0.75	0.60	−0.80	−0.60	0.25	−0.63	−0.53	0.24	−0.56
Aug	24.1	303.6	291.6	12.0	−0.83	0.59	−0.83	−0.59	0.10	−0.65	−0.70	0.23	−0.67
Sep	70.5	304.1	293.5	10.6	−0.82	0.47	−0.83	−0.52	0.02	−0.51	−0.52	0.16	−0.56
Oct	155.4	303.0	294.1	8.9	−0.79	0.13	−0.80	−0.09	−0.02	−0.08	0.07	0.13	−0.08
Nov	189.2	301.8	294.1	7.7	−0.78	0.12	−0.78	−0.28	−0.11	−0.21	−0.32	−0.18	−0.19
Dec	279.7	300.6	294.0	6.6	−0.74	0.10	−0.72	−0.20	0.06	−0.06	−0.29	0.10	−0.29

[a]Spatial correlation of LST with the PRODES forest cover product. For both products we used the mean of the years 2000–2005. Pixels with errors in land surface temperatures due to cloud contamination for all years (2000–2005) were excluded from the comparison with the PRODES forest cover product.
[b]Spatial correlation of the slope of LST with the slope of PRODES forest cover for the years 2000–2005. LST slopes were not calculated for cloud-contaminated pixels for the years 2000–2005. The influence of these errors on the slope is large because the data set covers only 6 years.
[c]Spatial correlation of the slope of LST with the *Hansen et al.* [2008] forest cover loss for the years 2000–2005.
[d]The 3B43 TRRM monthly accumulated surface rainfall (mm/month).

transpiration even as precipitation levels began to increase. The higher humidity levels for forest as compared with nonforest observed during September and October may decrease longwave cooling at night (as described above) and thus contribute to the smaller day-night LST differences observed during these months and during the following wet season.

[30] The correlation coefficients between PRODES forest cover and day LST, night LST, and day-night LST difference for the PRODES forest domain are given in Table 1. For each pixel we used the monthly means over 2000–2005 for LSTs and the annual means over 2000–2005 for the PRODES forest cover product. Pixels with missing or poor quality LST data for all years (2000–2005) were excluded from the comparison with PRODES, based on the quality flag in LST product MOD11B1. The highest correlations for day LST and day-night LST difference occurred at the end of the dry season (in August), while the highest correlation for night LST occurred a month earlier (July). Figures 4b, 4d, and 4f show the relationship between day LST, night LST, and day-night LST difference with the PRODES forest cover in August. For both the day LST and the day-night LST difference, a negative correlation of −0.83 was observed. Night LST had a positive correlation of 0.59 with forest cover. The relationship between land cover and LST was weaker during the wet season, with correlations in January, for example, of −0.69 for day LST, 0.14 for night LST, and −0.66 for the day-night LST difference.

3.2. LST and Forest Cover Change

[31] Moderate losses of forest cover were widely distributed in the north central part of Mato Grosso, to the west of Xingu Indigenous Reserve (Figures 2b and 2c). Figure 5 shows that some of the largest increases in day LST and day-night LST difference occurred in these areas. The map of change in night LST (Figure 5c) shows a more homogeneous pattern, with increases distributed widely in the southern part of the domain.

[32] Correlation coefficients between the change in forest cover during this period (forest fraction/yr) and the change in day LST, night LST, and day-night LST difference (K/yr) are shown in Table 1, for both the PRODES and *Hansen et al.* [2008] deforestation products. The LST slope was not calculated for cloud contaminated pixels, because the influence of these errors on the slope was large in our data set of only six years (2000–2005). During the 3 month period from January–March, 25437 out of 57600 pixels in our study area (44.2%) were contaminated. Contamination during the dry season, from July to September, was considerably lower (0.1%).

[33] The seasonal pattern of correlation for forest cover change was similar to that observed for forest cover: the highest correlations with the change in day LST and day-night LST difference occurred at end of the dry season in July and August for both the PRODES and *Hansen et al.* [2008] estimates. The correlation for night LST was highest during June and July for PRODES and July and August for *Hansen et al.* [2008], when precipitation was at or near minimum levels. In Figures 5b, 5d, and 5f the relationship between the change in LST and the change in PRODES forest cover are shown for the month of August. Both the change in day LST and day-night LST difference were negatively correlated with the changes in forest cover, with correlation coefficients of −0.59 and −0.65, respectively. While the day-night LST difference performed better than the day LST for predicting patterns of deforestation from PRODES, the reverse occurred for the *Hansen et al.* [2008] product, with correlations of −0.70 for day and −0.67 for the day-night LST difference. During other dry season months, however, including July and September, correlations with the day-night LST difference exceeded correlations with day LST for the *Hansen et al.* [2008] product (Table 1).

3.3. Feature Selection

[34] Correlations between the change in day and day-night LST difference and the change in forest cover were strongest during the dry season, and especially during the

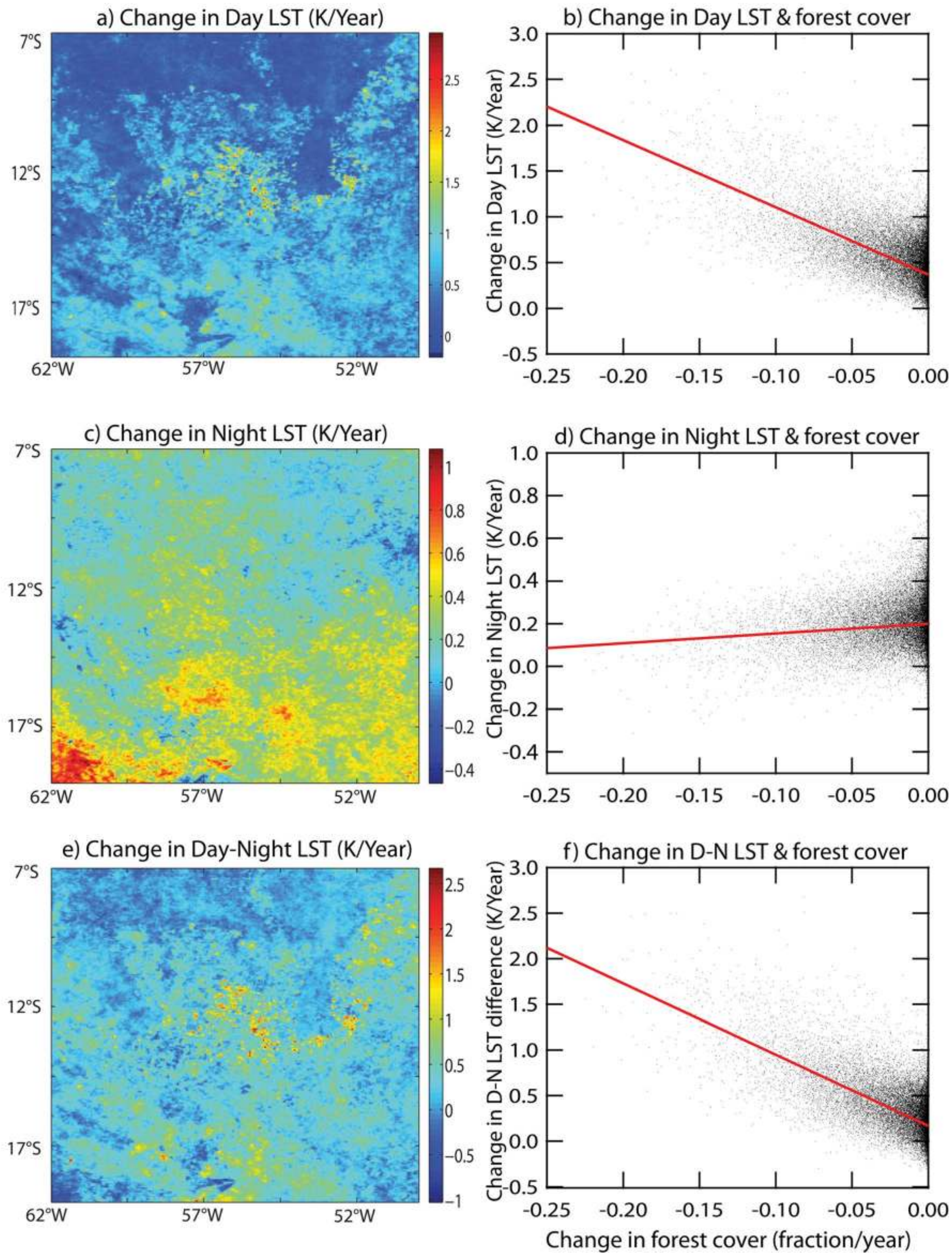

Figure 5. (left) Spatial distribution of the August (month of largest day-night LST difference) LST slope in unit K/yr from 2000 to 2005, for (a) daytime LST, (c) nighttime LST, and (e) day-night LST difference, and (right) the corresponding scatterplots against forest cover change from PRODES during 2000–2005. The results for linear regression fit (solid line) were: (b) for daytime LST, slope of −7.34, intercept of 0.37, and $p < 0.01$; (d) for nighttime LST, slope of 0.46, intercept of 0.20, and $p < 0.01$; (f) for day-night LST difference, slope of −7.80, intercept of 0.17, and $p < 0.01$. In total, 30436 pixels were used for the above regressions.

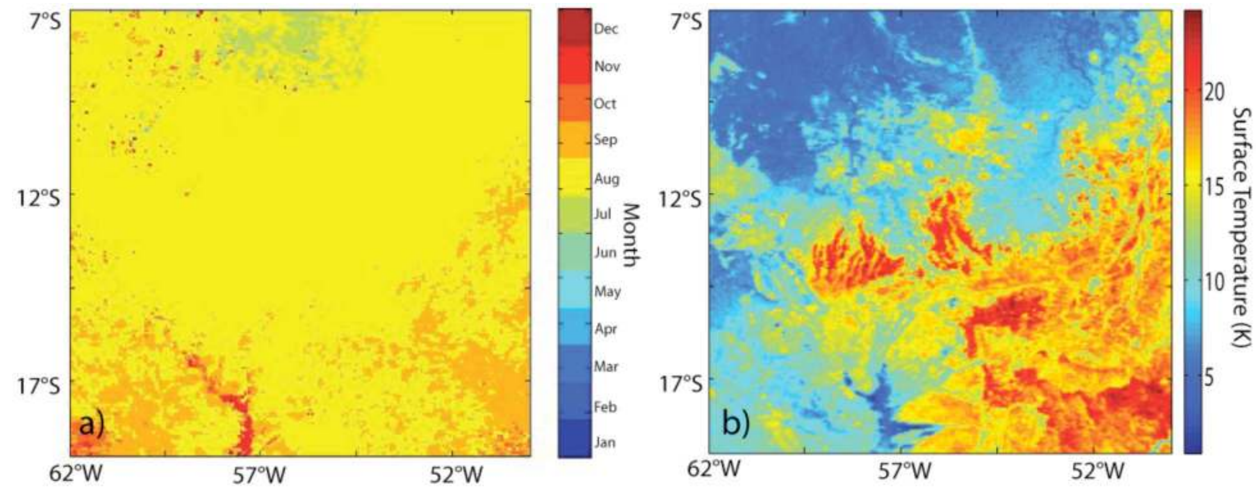

Figure 6. (a) The month corresponding to the maximum day and night land surface temperature difference for the study area. (b) The maximum monthly day-night land surface temperature difference (K) averaged over the years 2000–2005.

months of July, August, and September in Mato Grosso, as described above (section 3.2 and Table 1). To develop an approach that could be applied more widely across the tropics, we needed to develop an algorithm that could locally identify the seasonal period of the greatest drought stress. To find this period, we identified the period of maximum day-night LST difference in each grid cell, since Table 1 shows that during the months with the highest correlations between LST and PRODES and *Hansen et al.* [2008] forest cover change, the difference between day and night LST is the largest. First, we used all available observations from our 2000–2005 time series to construct a monthly mean annual cycle of day-night LST difference at each pixel. In a second step we found the monthly maximum day-night LST difference from this climatology, and its corresponding month. This month was defined as the center of a 3 month window that we then used to sample and calculate the 3 month averages of satellite products for our logistic regression model, including day LST, night LST, day-night LST difference, and NDVI.

[35] Using the above described feature selection method, the correlation coefficients showed a small improvement over the fixed monthly correlation coefficients shown in Table 1. For the correlation with PRODES forest cover, our algorithm showed correlation coefficients of −0.83 for day LST, 0.56 for night LST and −0.84 for day-night LST difference. The correlation coefficients with forest cover change were −0.67 and −0.71 (day LST), 0.12 and 0.25 (night LST) and −0.68 and −0.70 (day-night LST difference) for PRODES and *Hansen et al.* [2008] products, respectively. Figure 6a shows the month of maximum day-night LST difference for the study area, the state of Mato Grosso. For most pixels, this

Table 2. Logistic Regression Model Performance With Different Sets of Satellite Input Data

	Full Domain[a]		Active Deforestation Domain[b]	
Experiment	Correlation (r)	Area Predicted/Observed	Correlation (r)	Area Predicted/Observed
		LST Sampled During the Dry Season		
Day	0.58	1.51	0.58	2.48
Night	0.11	0.82	0.19	−1.09
Day-night	0.64	1.21	0.63	1.41
		D-N LST Sampled During Different Seasonal Periods		
Annual mean	0.48	0.97	0.58	−0.19
Wet season	0.05	1.79	0.08	0.40
		NDVI Sampled During Different Seasonal Periods		
Dry season[c]	0.80	1.23	0.78	1.24
Annual mean	0.66	1.41	0.66	0.93
Wet season[d]	−0.03	0.62	0.03	−1.68
		NDVI and D-N LST Sampled During Different Seasonal Periods		
Dry season	0.80	1.22	0.78	1.28
Annual mean	0.70	1.20	0.71	0.66
Wet season	0.02	1.85	0.07	−0.94

[a]The full domain corresponds to the area where PRODES data are available.
[b]The active deforestation domain corresponds to the pixels where PRODES predicted any deforestation.
[c]The dry season corresponds to the mean of a 3 month window, with the month of maximum day-night LST difference as center (see section 3.3).
[d]The wet season corresponds to the 3 month window that is exactly 6 months out of phase with the dry season.

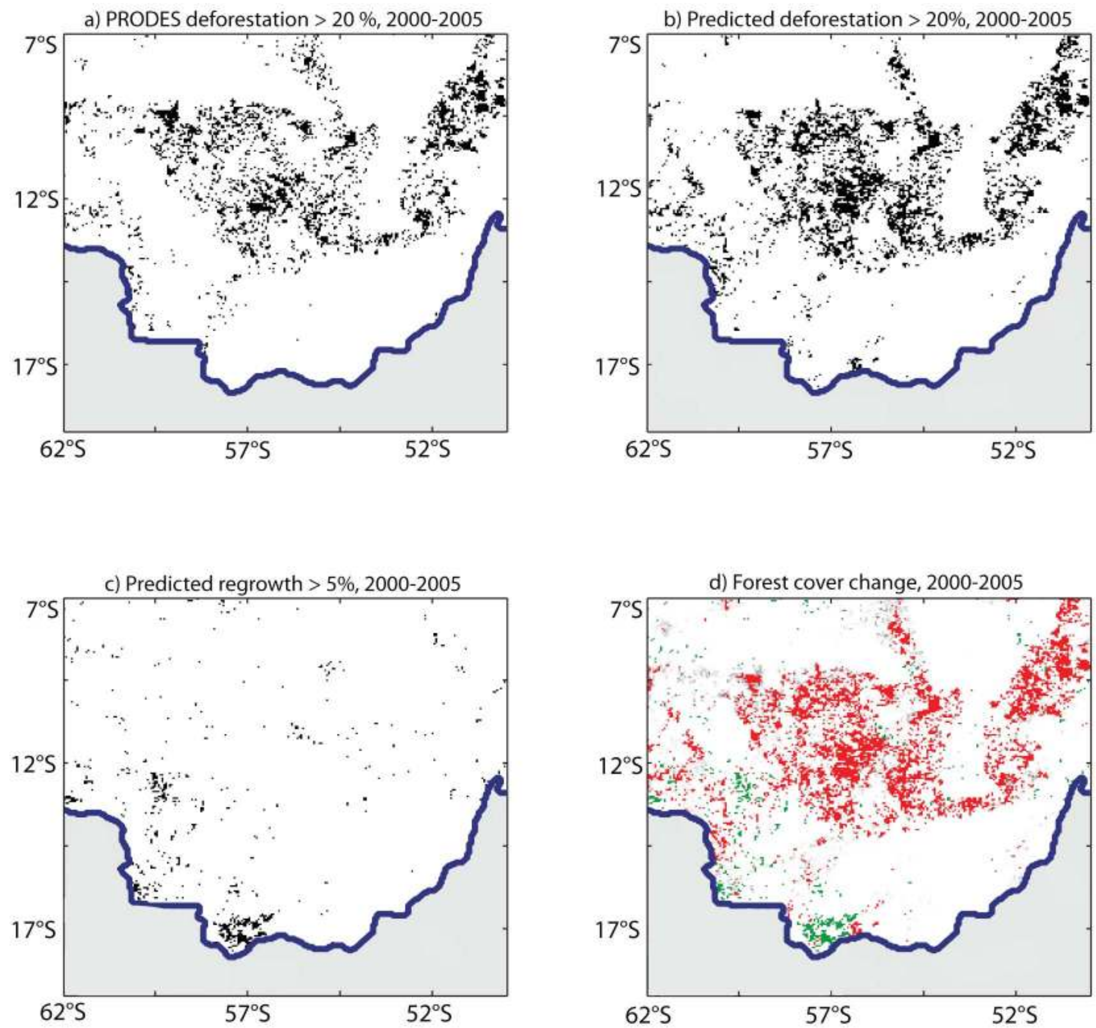

Figure 7. (a) Pixels in our study domain where PRODES showed more than 20% of deforestation between the years 2000 and 2005. Gray corresponds to the area outside the PRODES domain. (b) Pixels in our study domain where the NDVI and day-night LST difference sampled during the dry season predicted more than 20% deforestation between the years 2000 and 2005. (c) Pixels in our study domain where the NDVI and day-night LST difference sampled during the dry season predicted more than 5% of regrowth. (d) A map of the predicted deforestation and regrowth overlaid on the PRODES deforestation in our study area. Shown are the pixels where LST and NDVI, sampled during the dry season, predicted more than 20% of deforestation (red), pixels with more than 5% of predicted regrowth (green), and pixels where PRODES showed more than 20% deforestation but our algorithm predicted no or less than 20% deforestation (gray).

month corresponded to the end of the dry season (August). In the northern part of the study area there were some pixels where the maximum in day-night LST difference occurred 1 month earlier, whereas in the south many pixels reached a maximum later in the year, during September, October, and November. These differences can likely be explained by regional differences in climate. The maximum day-night LST is shown in Figure 6b. Large values were found in the southern part of the study area, whereas in the north and the wetlands of the Pantanal lower values were observed.

3.4. Logistic Regression Model Comparisons

[36] The performances of the logistic regression model to predict forest cover change for different experiments, as described in section 2.3, are shown in Table 2. We used different seasonal periods of satellite observations to construct the logistic regression models. The "dry season" corresponds to sampling the satellite observations according to the metric we developed in section 3.3. The wet season corresponded to a 3 month period that is exactly 6 months out of phase with the dry season window defined above, and the annual mean is simply the mean for all the months in a calendar year.

[37] For LSTs sampled during the dry season, the logistic regression model using the day-night LST difference performed better ($r = 0.64$) than the day LST ($r = 0.58$) or night LST ($r = 0.11$) models over the full domain. The ratio of the area of the predicted versus actual forest cover losses was

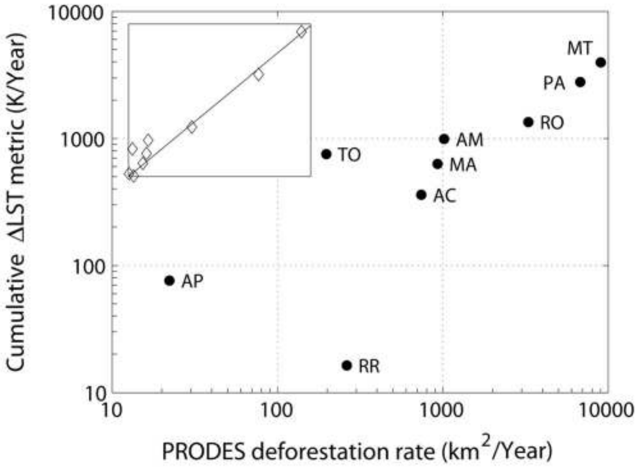

Figure 8. Comparison of cumulative day-night LST changes (in K/yr) with estimates of deforestation from PRODES (in km^2/yr) for states in the Brazilian Amazon during 2001–2005. The day-night LST changes were estimated as the slope of the day-night LST difference for each CMG grid cell sampled using our LST metric. Pixels with positive slopes and correlation coefficients larger than 0.7 (r) were summed within each state. The linear fit with PRODES data was described by a slope of 0.40, r equal to 0.98, and n equal to 9. Abbreviations are AC, Acre; AM, Amazonas; AP, Amapá; MA, Maranhão; MT, Mato Grosso; PA, Pará; RO, Rondônia; RR, Roraima; TO, Tocantins. Note that both *x* and *y* axis are plotted on a log scale.

1.21 for the day-night LST difference, indicating that the model was too sensitive to changes in the input features. Over the active deforestation part of the domain, the day-night LST difference model also had the highest correlation with observed forest cover loss. The ratio of predicted to observed forest cover loss was 1.41, and better than the ratio of the day LST (2.48) or night LST (−1.09). A ratio of 1 is ideal, so the day and day-night LST difference over-predicted forest cover loss in grid cells that PRODES identified as changing during 2000–2005. The negative ratio of −1.09 (night LST) corresponded to a prediction of more regrowth than deforested area.

[38] The use of information at the end of the dry season, when day-night LST was at maximum, substantially improved model predictions as compared with models using annual mean or wet season observations. This was true for models using day-night LST, NDVI, and both day-night LST and NDVI (Table 2). Models using annual mean observations showed the second best performance, with the correlation of 0.48 and a ratio of the predicted forest cover change over PRODES change of 0.97 in the whole domain. Models using wet season observations were substantially degraded.

[39] The predictions with NDVI showed a slightly better correlation than that with the day-night LST difference during the dry season, and the combination of the two sets of observations gave the same correlations (r = 0.80 for the full domain, and r = 0.78 for the active deforestation domain). Overall, the differences between the performance for the full domain and for only the active deforestation domain were small.

[40] The logistic regression model sampling the observations according to our algorithm (section 3.3) performed better than a model using observations from a fixed period during the dry season: August, the month of highest correlations between LST and PRODES forest cover (Table 1). The prediction using only August observations had a correlation coefficient with observed forest cover changes of 0.55 and 0.57 for day-night LST difference, 0.75 and 0.76 for NDVI, and 0.77 and 0.78 for the combination of NDVI and day-night LST difference (for the full and active deforestation domains, respectively).

[41] For predictions with the combined NDVI and day-night LST difference during the dry season, the spatial pattern of larger clearing areas (greater than 20% during 2000–2005) agreed reasonable well with PRODES (Figures 7a and 7b), although the logistic regression model predicted that the deforestation rate was somewhat higher than PRODES estimates in central part of Mato Grosso (9°S–13°S, 54°W–59°W).

[42] Besides detecting deforestation, we also used our algorithm to explore areas of savanna/forest regrowth. Because regrowth occurs over longer timescales than deforestation, we set the detection threshold in Figure 7 to a greater than 5% increase in fraction tree cover (compared to a greater than 20% decrease for deforestation). Areas where regrowth might occurred according to our algorithm were mostly confined to the savanna woodlands in the southwestern part of the PRODES domain (Figure 7c).

[43] Over our study period, climatic conditions (temperature and precipitation) that could also potentially explain increases in plant productivity, showed no trend. The areas of regrowth shown in Figure 7 may have been deforested prior to our study period. In past work, regrowth has sometimes been excluded from remote sensing studies using fractional tree cover to detect rates of deforestation [e.g., *Achard et al.*, 2002; *Hansen et al.*, 2008]. Our analysis suggests that changes in woodlands and savannas may also be contributing to global land use change carbon fluxes, although more work is needed with higher-resolution imagery and field measurements to verify these results and disentangle natural and anthropogenic causes of variability and trends in savanna structure and productivity.

3.5. Applicability of LST Metrics to Other Regions and Time Periods

[44] To check if our LST metric was applicable for areas other than the state of Mato Grosso, we compared cumulative LST changes with estimates from PRODES (available at

Table 3. Relationships Between Changes in Day-Night LST and PRODES or *Hansen et al.* [2008] Deforestation Rates

Region	Dry Season[a]	Annual Mean	Wet Season[b]
Legal Amazon[c]	0.98	0.88	0.37
Southeast Asia[d]	0.67	0.46	0.11

[a]The dry season corresponded to the mean of the 3 month window, centered on month of maximum day-night LST difference (see section 3.3).

[b]The wet season corresponded to the 3 month window that was exactly 6 months out of phase with the dry season.

[c]Aggregated values from nine Brazilian states were used to compute the correlation coefficient: Acre, Amazonas, Amapá, Maranhão, Mato Grosso, Pará, Rondônia, Roraima, and Tocantins.

[d]Six areas were used: Cambodia, Kalimantan, Malaysia, Sulawesi, Sumatra, and Thailand.

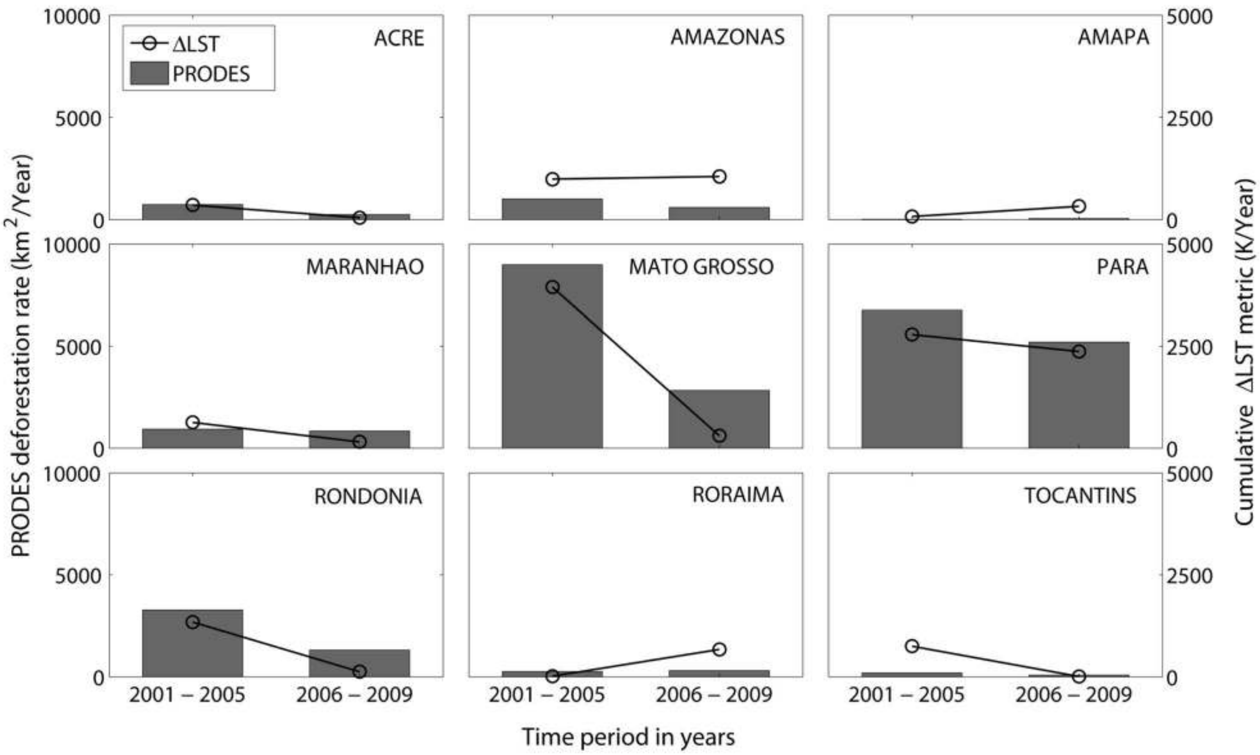

Figure 9. Time series of PRODES deforestation rate in km^2/yr (gray bars, *y* axis) and the cumulative change in day-night LST (in K/yr) within each region (solid black line, secondary *y* axis) for nine Brazilian states (years 2001–2005 and 2006–2009).

the INPE website: http://www.obt.inpe.br/prodes/) for all of the Brazilian states within the Amazon (Figure 8). Cumulative LST changes were estimated as the slope of the day-night LST difference for the years 2000–2005 sampled using our grid cell specific approach for identifying the dry season. For each state, we took the sum of all pixels within each spatial domain that had a positive slope and a correlation coefficient larger than 0.7.

[45] In Table 3 we report the statistics for our day-night LST metric and for day-night LST changes derived using either annual mean or the 6 month out of phase observations. We also show the results for different countries in Southeast Asia, based on a comparison with the global deforestation product from *Hansen et al.* [2008] for the years 2000–2005. Although the spatial correlations of the regression were not as good as for the states across the Brazilian Amazon, a clear improvement occurred when day-night LST was sampled during the local dry season (i.e., during the seasonal period when the day-night LST differences were most pronounced).

[46] In Figure 9 we compare the PRODES deforestation rate in km^2/yr with our day-night LST metric described above for two periods: 2001–2005 and 2006–2009. The day-night LST changes decreased during 2006–2009 relative to 2001–2005 for many states within the Amazon, providing an independent confirmation of lower deforestation levels during the latter part of this decade as reported by PRODES. For the states which are important from a deforestation perspective (Mato Grosso, Pará, Rondônia), we observed large decreases in the day-night LST metric for the 2006–2009 period.

4. Discussion

[47] Our analysis suggests that information from thermal bands can be useful in monitoring deforestation; especially when sampled during the dry season and when day and night LST observations are combined. Logistic regression models of forest cover change using LST sampled in this way were slightly less effective than models using NDVI, but they performed well enough to be useful when NDVI data for a region is unavailable or noisy. LST observations may be particularly useful with satellite spectrometers that do not have high-resolution spectral bands that allow for estimation of NDVI (e.g., Geostationary Operational Environmental Satellite (GOES)), or in areas where aerosols limit the usefulness of visible and near-infrared surface reflectance observations.

[48] The information content of LST data varied considerably from season to season. High correlations between day-night LST difference data and PRODES and *Hansen et al.* [2008] forest cover change were observed at the end of the dry season (August in our study area and approximately 1–2 months after minimum monthly precipitation). In contrast, during the wet season the correlations were significantly lower. The higher amount of cloud-

contaminated pixels in the wet months like December, January, and February might have played a role here. Even during periods without cloud cover, increases in column water vapor content during the wet season likely contributed to smaller differences in nighttime cooling between forest and nonforest areas (e.g., Figure 3). Higher correlations were found in the months when cloud contamination and precipitation were low, surface humidity was at a minimum, and the difference between day and night LST was the largest. We found large variations in the correlations between LST data and forest cover change during the year. Therefore, it is important that the use of LST data in deforestation classifiers take advantage of seasonal periods with the highest descriptive power. To predict these months, we developed a simple temporal sampling algorithm based on the largest day-night LST difference. Different tests showed that data based on the LST during a 3 month window centered on the month derived from this metric yielded the highest correlations with independent data.

[49] Besides the importance of the temporal sampling of LST data, our analysis showed that during the end of the dry season the day-night LST difference performed better than the day LST for comparisons we made with PRODES; several experiments in our logistic regression model confirmed this. On the other hand, a comparison with *Hansen et al.* [2008] forest cover loss data showed slightly higher correlations for the day LST than the day-night difference during August (but the reverse in July and September). The reasons for the different performance of day-night LST differences with PRODES and *Hansen et al.* [2008] deforestation products remain unclear and will require further analysis with higher spatial resolution LST data. Day LST has already been used in different deforestation classifiers; the approach of using the day-night LST difference data in deforestation classifiers is novel and may reduce the sensitivity of LST-based approaches to interannual variability in climate and to variations in topography. Effects of climate change and topography are expected to influence both day and night LSTs in the same direction, so day-night LST differences may be less sensitive to these factors. This reduced sensitivity may be of particular use in constructing long time series of land cover change that extend across multiple satellites, including those that have different sensor characteristics.

[50] A disadvantage of using the day-night LST difference as compared to day LST is that the day-night LST difference may be more sensitive to cloud contamination because two, rather than one, clear-sky images are needed to construct this metric and because cloud cover may be higher in tropical regions at night [*Durieux et al.*, 2003]. During the dry season, and especially the months of July, August, and September, day and night LST products from MODIS had more cloud-free observations than during other periods. As described above, lower water content in the atmospheric column also probably allows for greater nighttime cooling and thus the potential for greater discrimination between high and low stature vegetation. Thus, sampling LST during the end of the dry season using the algorithm we developed may have advantages considering both surface biophysical and atmospheric contamination perspectives. In future work, by combining Aqua and Terra observations (with up to four overpasses per day) it may be possible to partly resolve some of issues related to cloud contamination.

[51] The region of focus for this study was in the arc of deforestation in the state of Mato Grosso, Brazil. Deforestation and climatic characteristics in this region are well suited for MODIS-based deforestation monitoring, because long dry seasons and low-stature transition forest types enable the mechanized clearing of forest cover [*Morton et al.*, 2005]. These large clearings are more easily detected with moderate resolution remote sensing products, and cloud cover is much lower during the dry season, increasing the chance for cloud-free MODIS imagery. In other important humid tropical regions in Africa and Asia the dry season is considerably weaker, limiting cloud-free imagery [*Hansen et al.*, 2009], and also the sizes of tropical forest clearings may be smaller than those that typically occur in Mato Grosso, Brazil. Large mechanized clearings are used for the creation of pastures and croplands in Mato Grosso [*Morton et al.*, 2006], whereas clearings in Asia and especially Africa are smaller in size and associated with logging activities and smaller-scale agricultural complexes.

[52] Although some results of our LST metric in other areas (Brazilian Amazon and Southeast Asia) were promising (Figures 8 and 9), more work with higher-resolution LST data is needed to assess whether our approach will be useful in regions that have smaller clearing sizes. In principal, subpixel changes in forest cover should impart changes in LST that are detectable in moderate resolution observations; the linearity of these responses are not well understood and require further study.

[53] Use of the coarse resolution climate modeling grid (CMG) products here was a useful first step for evaluating the information content of different LST measurements as a function of overpass time and monthly sampling interval. An important next step toward the development of an operational pantropical forest classifier is to assess the performance of these different types of observations with 1 km MODIS LST data, 90 m Advanced Spaceborne Thermal Emission and Reflection Radiometer (ASTER) observations, and in future, with 60 m observations from the planned Hyperspectral Infrared Imager (HyspIRI) Mission. Higher-resolution LST data also are likely to be more effective in identifying the exact geographic location of deforestation. MODIS LST data are appropriate for rapid identification of the location of deforestation areas and trends in deforestation dynamics, but cannot be seen as a replacement for higher-resolution systems based on Landsat and other higher-resolution surface reflectance imagery.

5. Conclusions

[54] LST data can be a useful information source in classification models for distinguishing between forest and nonforest areas and for quantifying deforestation in a continuous way. The information content of the day LST and day-night LST difference observations varied considerably over an annual cycle. At the end of the dry season, when precipitation was low, surface humidity was at a minimum, and the difference between day and night LST was large, the highest correlations were found with the PRODES and *Hansen et al.* [2008] forest cover change in the Brazilian state of Mato Grosso. Based on this analysis, we developed a metric to monitor forest cover change in the humid tropics. Besides the importance of sampling LST data during the

months with the highest descriptive power, we found that the day-night LST difference in general improved the ability of classification models to distinguish forest and nonforest areas as compared with models that only use day LST. We were able to show using this approach that changes in day-night LSTs were highly correlated with the spatial pattern of deforestation across different Brazilian states within the Amazon. Changes in day-night LSTs were lower within the Amazon during 2006–2009 relative to 2001–2005, providing independent confirmation of decreases in the rate of deforestation during the latter part of this decade as reported by PRODES.

[55] Further research is needed to optimize our day-night LST difference algorithm in detecting tropical forest cover change; the use of higher spatial and temporal resolution LST data needs to be explored, because the actual clearing size of forest in often smaller than the pixel size of the coarse resolution (0.05° × 0.05°) LST data used in this study. Longer time series of LST from MODIS, that now extend over a decade in length, may increase our ability to use LST observations in effective ways to detect long-term changes in forest cover. Next steps are to validate this approach using higher-resolution Landsat observations and to extend this approach globally.

[56] **Acknowledgments.** This work was supported by NASA grants NNX08AF64G, NNX08AG13G, and NNX08AR69G, and NSF grant IIS-0431085. We obtained the MODIS observations from the Land Processes Distributed Active Archive Center (LP DAAC) located at the U.S. Geological Survey (USGS) Earth Resources Observation and Science (EROS) Center (https://lpdaac.usgs.gov).

References

Achard, F., et al. (2002), Determination of deforestation rates of the world's humid tropical forests, *Science*, *297*(5583), 999–1002, doi:10.1126/science.1070656.

Achard, F., et al. (2007), Pan-tropical monitoring of deforestation, *Environ. Res. Lett.*, *2*, 045022, doi:10.1088/1748-9326/2/4/045022.

Anderson, L. O., et al. (2005), Assessment of deforestation in near real time over the Brazilian Amazon using multitemporal fraction images derived from terra MODIS, *IEEE Geosci. Remote Sens. Lett.*, *2*(3), 315–318, doi:10.1109/LGRS.2005.850364.

Andreux, F. G., and C. C. Cerri (1989), Current trends in the research on soil changes due to deforestation, burning and cultivation in the Brazilian tropics, *Toxicol. Environ. Chem.*, *20*(1), 275–283, doi:10.1080/02772248909357387.

Aumann, H. H., et al. (2003), AIRS/AMSU/HSB on the aqua mission: Design, science objectives, data products, and processing systems, *IEEE Trans. Geosci. Remote Sens.*, *41*(2), 253–264, doi:10.1109/TGRS.2002.808356.

Bala, G., et al. (2007), Combined climate and carbon-cycle effects of large-scale deforestation, *Proc. Natl. Acad. Sci. U. S. A.*, *104*(16), 6550–6555, doi:10.1073/pnas.0608998104.

Borak, J. S., E. F. Lambin, and A. H. Strahler (2000), The use of temporal metrics for land cover change detection at coarse spatial scales, *Int. J. Remote Sens.*, *21*, 1415–1432, doi:10.1080/014311600210245.

Bruno, R. D., et al. (2006), Soil moisture dynamics in an eastern Amazonian tropical forest, *Hydrol. Process.*, *20*(12), 2477–2489, doi:10.1002/hyp.6211.

Canadell, J. G., et al. (2007), Contributions to accelerating atmospheric CO_2 growth from economic activity, carbon intensity, and efficiency of natural sinks, *Proc. Natl. Acad. Sci. U. S. A.*, *104*(47), 18,866–18,870, doi:10.1073/pnas.0702737104.

Carlson, T., and R. Gillies (1994), A method to make use of thermal infrared temperature and NDVI measurements to infer surface soil water content and fractional vegetation cover, *Remote Sens. Rev.*, *9*, 161–173.

Carreiras, J. M. B., et al. (2002), Fraction images derived from SPOT-4 VEGETATION data to assess land-cover change over the state of Mato Grosso, Brazil, *Int. J. Remote Sens.*, *23*(23), 4979–4983, doi:10.1080/01431160210000016743.

Collatz, G. J., et al. (2000), A mechanism for the influence of vegetation on the response of the diurnal temperature range to changing climate, *Geophys. Res. Lett.*, *27*(20), 3381–3384, doi:10.1029/1999GL010947.

Davidson, E. A., et al. (2007), Recuperation of nitrogen cycling in Amazonian forests following agricultural abandonment, *Nature*, *447*, 995–998, doi:10.1038/nature05900.

DeFries, R. S., and J. R. G. Townshend (1994), NDVI-derived land-cover classifications at a global scale, *Int. J. Remote Sens.*, *15*(17), 3567–3586, doi:10.1080/01431169408954345.

DeFries, R. S., et al. (1995), Mapping the land surface for global atmosphere-biosphere models: Toward continuous distributions of vegetation's functional properties, *J. Geophys. Res.*, *100*(D10), 20,867–20,882, doi:10.1029/95JD01536.

DeFries, R. S., et al. (2000), Global continuous fields of vegetation characteristics: A linear mixture model applied to multi-year 8 km AVHRR data, *Int. J. Remote Sens.*, *21*(6–7), 1389–1414, doi:10.1080/014311600210236.

DeFries, R. S., et al. (2002), Carbon emissions from tropical deforestation and regrowth based on satellite observations for the 1980s and 1990s, *Proc. Natl. Acad. Sci. U. S. A.*, *99*(22), 14,256–14,261, doi:10.1073/pnas.182560099.

DeFries, R. S., et al. (2004), Land-use choices: Balancing human needs and ecosystem function, *Front. Ecol. Environ*, *2*(5), 249–257, doi:10.1890/1540-9295(2004)002[0249:LCBHNA]2.0.CO;2.

DeFries, R., et al. (2007), Earth observations for estimating greenhouse gas emissions from deforestation in developing countries, *Environ. Sci. Policy*, *10*, 385–394, doi:10.1016/j.envsci.2007.01.010.

Durieux, L., L. A. T. Machado, and H. Laurent (2003), The impact of deforestation on cloud cover over the Amazon arc of deforestation, *Remote Sens. Environ.*, *86*, 132–140, doi:10.1016/S0034-4257(03)00095-6.

Eidenshink, J. C., and J. L. Faundeen (1994), The 1 km AVHRR global land data set—1st stages in implementation, *Int. J. Remote Sens.*, *15*(17), 3443–3462, doi:10.1080/01431169408954339.

Foley, J. A., et al. (2005), Global consequences of land use, *Science*, *309*(5734), 570–574, doi:10.1126/science.1111772.

Food and Agriculture Organization (2006), Global Forest Resources Assessment 2005, *FAO For. Pap. 147*, U. N., Rome.

Friedl, M. A. (2002), Forward and inverse modeling of land surface energy balance using surface temperature measurements, *Remote Sens. Environ.*, *79*(2–3), 344–354, doi:10.1016/S0034-4257(01)00284-X.

Friedl, M. A., and C. E. Brodley (1997), Decision tree classification of land cover from remotely sensed data, *Remote Sens. Environ.*, *61*(3), 399–409, doi:10.1016/S0034-4257(97)00049-7.

Friedl, M. A., et al. (2002), Global land cover mapping from MODIS: Algorithms and early results, *Remote Sens. Environ.*, *83*(1–2), 287–302, doi:10.1016/S0034-4257(02)00078-0.

Goetz, S. J., et al. (2009), Mapping and monitoring carbon stocks with satellite observations: A comparison of methods, *Carbon Balance Manag.*, *4*(2), doi:10.1186/1750-0680-4-2.

Gopal, S., and C. Woodcock (1996), Remote sensing of forest change using artificial neural networks, *IEEE Trans. Geosci. Remote Sens.*, *34*(2), 398–404, doi:10.1109/36.485117.

Goulden, M. L., et al. (2006), Nocturnal cold air drainage and pooling in a tropical forest, *J. Geophys. Res.*, *111*, D08S04, doi:10.1029/2005JD006037.

Hamilton, L. S., and P. N. King (1983), *Tropical Forested Watersheds: Hydrologic and Soils Response to Major Uses or Conversions*, pp. 137–168, Westview, Boulder, Colo.

Hansen, M. C., and R. S. DeFries (2004), Detecting long-term global forest change using continuous fields of tree-cover maps from 8-km advanced very high resolution radiometer (AVHRR) data for the years 1982–99, *Ecosystems*, *7*(7), 695–716, doi:10.1007/s10021-004-0243-3.

Hansen, M. C., et al. (2000), Global land cover classification at 1km spatial resolution using a classification tree approach, *Int. J. Remote Sens.*, *21*(6–7), 1331–1364, doi:10.1080/014311600210209.

Hansen, M. C., et al. (2008), Humid tropical forest clearing from 2000 to 2005 quantified by using multitemporal and multiresolution remotely sensed data, *Proc. Natl. Acad. Sci. U. S. A.*, *105*(27), 9439–9444, doi:10.1073/pnas.0804042105.

Hansen, M. C., et al. (2009), Quantifying changes in the rates of forest clearing in Indonesia from 1990 to 2005 using remotely sensed data sets, *Environ. Res. Lett.*, *4*(3), 034001, doi:10.1088/1748-9326/4/3/034001.

Holben, B. (1986), Characteristics of maximum-value composite images from temporal AVHRR data, *Int. J. Remote Sens.*, *7*, 1417–1434, doi:10.1080/01431168608948945.

Hosmer, D. W., and S. Lemeshow (2004), *Applied Logistic Regression*, Wiley, New York.

Houghton, R. A. (1991), Tropical deforestation and atmospheric carbon-dioxide, *Clim. Change*, *19*(1–2), 99–118, doi:10.1007/BF00142217.

Houghton, R. A., et al. (2000), Annual fluxes or carbon from deforestation and regrowth in the Brazilian Amazon, *Nature*, *403*(6767), 301–304, doi:10.1038/35002062.

Huete, A. R., et al. (2002), Overview of the radiometric and biophysical performance of the vegetation indices, *Remote Sens. Environ.*, *83*(1–2), 195–213, doi:10.1016/S0034-4257(02)00096-2.

Instituto Nacional de Pesquisas Espaciais (INPE) (2002), Deforestation estimates in the Brazilian Amazon, São José dos Campos, Minist. da Ciênc. e Tecnol., Brasilia. (Available at <http://www.obt.inpe.br/prodes/)>

Jasinski, E., et al. (2005), Physical landscape correlates of the expansion of mechanized agriculture in Mato Grosso, Brazil, *Earth Interact.*, *9*, 1–18, doi:10.1175/EI143.1.

Kummerow, C., et al. (1998), The Tropical Rainfall Measuring Mission (TRMM) sensor package, *J. Atmos. Oceanic Technol.*, *15*(3), 809–817, doi:10.1175/1520-0426(1998)015<0809:TTRMMT>2.0.CO;2.

Lambin, E. F., and D. Ehrlich (1995), The vegetation indices and surface temperature for land-cover mapping at broad spatial scales, *Int. J. Remote Sens.*, *16*, 573–579, doi:10.1080/01431169508954423.

Los, S. O., et al. (1994), A global 1-degree-by-1-degree NDVI data set for climate studies derived from the GIMMS continental NDVI data, *Int. J. Remote Sens.*, *15*(17), 3493–3518, doi:10.1080/01431169408954342.

Mildrexler, D. J., et al. (2007), A new satellite-based methodology for continental-scale disturbance detection, *Ecol. Appl.*, *17*(1), 235–250, doi:10.1890/1051-0761(2007)017[0235:ANSMFC]2.0.CO;2.

Morton, D. C., et al. (2005), Rapid assessment of annual deforestation in the Brazilian Amazon using MODIS data, *Earth Interact.*, *9*, 1–22, doi:10.1175/EI139.1.

Morton, D. C., et al. (2006), Cropland expansion changes deforestation dynamics in the southern Brazilian Amazon, *Proc. Natl. Acad. Sci. U. S. A.*, *103*(39), 14,637–14,641, doi:10.1073/pnas.0606377103.

Nabuurs, G. J., et al. (2007), Forestry, in *Climate Change 2007: Mitigation. Contribution of Working Group III to the Fourth Assessment Report of the Intergovernmental Panel on Climate Change*, edited by B. Metz et al., pp. 547–561, Cambridge Univ. Press, Cambridge, U. K.

Nelder, J. A., and R. W. M. Wedderburn (1972), Generalized linear models, *J. R. Stat. Soc. A*, *135*, 370–384.

Nemani, R. R., and S. W. Running (1997), Land cover characterization using multitemporal red, near-IR, and thermal-IR data from NOAA/AVHRR, *Ecol. Appl.*, *7*, 79–90, doi:10.1890/1051-0761(1997)007[0079:LCCUMR]2.0.CO;2.

Nemani, R., et al. (1993), Developing satellite-derived estimates of surface moisture status, *J. Appl. Meteorol.*, *32*(3), 548–557, doi:10.1175/1520-0450(1993)032<0548:DSDEOS>2.0.CO;2.

Nobre, C. A., et al. (1991), Amazonian deforestation and regional climate change, *J. Clim.*, *4*(10), 957–988, doi:10.1175/1520-0442(1991)004<0957:ADARCC>2.0.CO;2.

Pongratz, J., et al. (2006), The impact of land cover change on surface energy and water balance in Mato Grosso, Brazil, *Earth Interact.*, *10*, 1–17, doi:10.1175/EI176.1.

Price, J. C. (1984), Land surface temperature measurements from the split window channels of the NOAA 7 advanced very high resolution radiometer, *J. Geophys. Res.*, *89*(D5), 7231–7237, doi:10.1029/JD089iD05p07231.

Roy, D. P., P. Kennedy, and S. Folving (1997), Combination of the Normalized Difference Vegetation Index and surface temperature for regional scale European Forest cover mapping using AVHRR data, *Int. J. Remote Sens.*, *18*, 1189–1195, doi:10.1080/014311697218665.

Sala, O. E., et al. (2000), Biodiversity: Global biodiversity scenarios for the year 2100, *Science*, *287*(5459), 1770–1774, doi:10.1126/science.287.5459.1770.

Salomonson, V. V., et al. (1989), MODIS: Advanced facility instrument for studies of the Earth as a system, *IEEE Trans. Geosci. Remote Sens.*, *27*(2), 145–153, doi:10.1109/36.20292.

Shimabukuro, Y. E., et al. (1998), Vegetation index and spectral linear mixing model for monitoring the Pantanal region, *Pesquisa Agropecu. Bras.*, *33*, 1729–1737.

Shukla, J., et al. (1990), Amazon deforestation and climate change, *Science*, *247*(4948), 1322–1325, doi:10.1126/science.247.4948.1322.

Smith, R. C. G., and B. J. Choudhury (1991), Analyses of normalized difference and surface temperature observations over southeastern Australia, *Int. J. Remote Sens.*, *12*, 2021–2044, doi:10.1080/01431169108955234.

United Nations Framework Convention for Climate Change (2005), Eleventh Conference of Parties (COP), Agenda item 6: Reducing emissions from deforestation in developing countries, Geneva, Switzerland.

Wan, Z., Y. Zhang, Q. Zhang, and Z. L. Li (2002), Validation of the land-surface temperature products retrieved from Terra Moderate Resolution Imaging Spectroradiometer data, *Remote Sens. Environ.*, *83*, 163–180, doi:10.1016/S0034-4257(02)00093-7.

A. J. Frank and P. Smyth, Department of Computer Science, University of California, Donald Bren Hall, Irvine, CA 92697, USA. (ajfrank@ics.uci.edu; smyth@ics.uci.edu)

M. L. Goulden, Y. Jin, and J. T. Randerson, Department of Earth System Science, University of California, Croul Hall, Irvine, CA 92697, USA. (mgoulden@uci.edu; yufang@uci.edu; jranders@uci.edu)

G. R. van der Werf and T. T. van Leeuwen, Department of Hydrology and Geo-environmental Sciences, VU University Amsterdam, De Boelelaan 1085, NL-1081 HV Amsterdam, Netherlands. (guido.van.der.werf@falw.vu.nl; thijs.van.leeuwen@falw.vu.nl)